

TIME AND FREQUENCY DOMAIN WAVE PROPAGATORS

Funda Akleman¹ Levent Sevgi^{2,3}

¹*ITU Electronics and Communication Engineering Department,
80626 Maslak / Istanbul, TURKEY*

²*ITU Institute of Science and Technology, Defense Technologies,
80626 Maslak / Istanbul, TURKEY*

³*TUBITAK-Marmara Research Center, Electronic Systems Department
Gebze / Kocaeli TURKEY*

Abstract - *In this paper, a new time-domain wave propagator (TDWP) that was recently introduced, is compared against a frequency-domain one that has been in use for more than a decade. The new time-domain wave propagator is built by a two-dimensional (2D) finite-difference time-domain (FDTD) algorithm. The frequency-domain wave propagator is the Split-step Parabolic Equation (SSPE), which is the solution of (one-way) wave equation in parabolic form. These two techniques can be both used for different kinds of 2D propagation problems. In this paper, ground wave problems, which are difficult to solve, have been taken into consideration in order to compare the methods and show their power. Assuming an azimuthal symmetry, ground wave propagation and surface and/or elevated ducts may be represented via transverse and/or longitudinal refractivity and boundary perturbations in 2D space. The 2D propagation space extends from $x=0$ (bottom) to $x \rightarrow \infty$ (top), vertically and from $z \rightarrow -\infty$ (left) to $z \rightarrow \infty$ (right), horizontally. Pulse propagation is simulated in TDWP and while a moving window escorts the transmitted waveform from one end to the other end within the FDTD computation space, time histories are accumulated at chosen observation points. Any vertical and/or horizontal field profile at a desired frequency is extracted by applying off-line discrete Fourier transformation (DFT). On the other hand, a given vertical field profile is longitudinally propagated by moving back and forth between the transverse spatial and wavenumber domains in SSPE. The results of TDWP and SSPE are compared on different ducting and anti-ducting refractivity profiles and their agreement is presented.*

I. Introduction

Today's communication systems as well as radars are mostly used within multi-area, multi-sensor, land-based, maritime and/or air-based integrated complex systems (such as an integrated maritime surveillance system or integrated early warning system against tactical ballistic missiles, etc.). The research towards development and, then, to the performance evaluations of such systems require powerful computer simulation tools and can only be done via these simulators. Some requirements related to current integrated system simulations are as follows:

- Modeling of propagation characteristics and path loss predictions in integrated surveillance systems, where microwave as well as HF (high-frequency) radars are used,
- Service planning, in rural and urban locations for mobile communication systems using both 900MHz and 1.8GHz systems
- Knowledge of propagation characteristics to overcome problems related to emerging radar technologies (HF and VHF radars).

All these simulations require the simulation of ground wave propagation through atmosphere over a 3D regional digitized terrain map. A service planner, site-engineer or the leader of a small military ground contingent needs to have access in real time to the propagation characteristics between any two selected points (e.g., a communication transmitter and receiver) including terrain profile, vegetation and atmospheric effects. It has been a continuing challenge to prepare a general chart or computer code to satisfy such requirements.

Although all physical propagation problems are in three dimensions (3D), two dimensional (2D) approximations can be used if symmetry in one of the three dimensions exists or is assumed to exist. It is well accepted to solve atmospheric propagation problems in 2D for a broad frequency range because of the approximate azimuthal symmetry of earth. It is also common to use 2D solutions in some optical propagation problems (e.g. slab waveguide propagation solutions). Here, communication problems that involve atmospheric propagation are taken into account.

Long range communication, which includes both ground and sky waves, is one of the most difficult and important propagation problems. Sky wave is mostly affected by the upper atmosphere (ionosphere), while ground wave propagation changes due to the lower and middle atmosphere (troposphere) characteristics as well as ground effects. In this paper, ground wave propagation that can be solved by split step parabolic equation (SSPE) and time domain wave propagator (TDWP), is taken into consideration.

Ground waves have three components: direct waves, ground-reflected waves and surface waves. The model environment is a spherical earth with various ground characteristics, above which exists a radially inhomogeneous atmosphere. Having an excitation and observer anywhere on or above the ground, this model has served as a canonical problem. This problem is very complex and a full-wave, numerically computable analytical solution has not appeared yet. The physical characteristics of the propagation depend on many parameters, such as the operating frequency, medium parameters, transmitter and receiver locations and the geometry (boundary conditions, BC) between them. For example, the propagation is limited by the line-of-sight at microwaves because surface waves are almost negligible at these frequencies. On the other hand, beyond the horizon propagation is possible at HF (3-30MHz) and lower frequencies, because surface waves may reach ranges up to hundreds of kilometers in diffraction region.

Ground wave propagation problem and available analytical approximate solutions have been outlined in [1] together with the hybridization of ray and mode methods. Some of analytical-numerical and pure numerical techniques have also been summarized in [1]. Surface and/or elevated-ducting effects of various transverse as well as longitudinal refractivity profiles have been investigated either analytically [2-5], or numerically [6-8].

Here, two different wave propagators, which simulate wave propagation in time and frequency domains, are taken into account. The first one, TDWP, has been recently introduced and is a general technique that can be applied to broad range of propagation problems [9]. It is based on a two-dimensional (2D) finite-difference time-domain [10] (FDTD) algorithm, where broad band pulse propagation is simulated and traced over long distances by a virtual rectangular window that circulates the FDTD space longitudinally back and forth until the range of interest is reached. The second one, SSPE, is the well-known split step parabolic equation technique, which is the solution of one-way wave equation in parabolic form [6-8]. In Sec.II, FDTD based TDWP is briefly summarized. The classical SSPE wave propagator is outlined in Sec.III. Numerical examples are chosen to be the simulations of wave propagation through surface guiding and anti-guiding ducts and are presented

in Sec.IV, where results of the two techniques are compared. Finally, the conclusions and future implementations that are needed are given in Sec.V.

II. The Time-domain Wave Propagator (TDWP)

The 2D-FDTD wave propagation region and the FDTD computation space are pictured in Fig.1. The structure is assumed to have an azimuthal symmetry. The transverse (x) and longitudinal (z) field components are E_x , H_y and E_z , respectively, which models the classical 2D TM_z ground wave propagation over earth's surface, representing a vertical polarization problem.

FDTD is based on the discretization of Maxwell's two curl equations directly in time and spatial domains and dividing the volume of interest into very small identical blocks called Yee cells [10]. In 3D-FDTD, there are three electric and three magnetic field components in each Yee cell distinguished by (i,j,k) label. The time and spatial discretization steps are Δt and Δx , Δy , Δz , respectively. Although field components in each cell are labeled with the same (i,j,k) numbers (such as $E_x(i,j,k)$ or $H_z(i,j,k)$), their locations are different. There is also a $\Delta t/2$ time difference between E and H field components in the Yee cell. Any object may be simulated by the medium parameters permittivity ϵ [F/m], permeability μ [H/m] and conductivity σ [S/m]. Although electric and magnetic field components are updated during the time simulation, voltages and currents in (i,j,k) cell may be obtained directly from Gauss and Faraday laws. Narrow and broad band responses may be readily obtained via FDTD simulations. Since its first introduction, other algorithms, such as free-space simulations (i.e., absorbing boundary simulations) and near-to-far field transformations have supported FDTD. Now, FDTD can be applied to variety of complex electromagnetic problems including radar cross-section (RCS) prediction and antenna simulations [11,12], biomedical modeling [13] and planar microwave network analysis and electromagnetic compatibility (EMC) simulations [14].

In TDWP, the related iterative FDTD equations are

$$E_x^n(i, k) = \frac{\epsilon}{\epsilon + \sigma \Delta t} E_x^{n-1}(i, k) - \frac{\Delta t}{(\epsilon + \sigma \Delta t) \Delta z} [H_y^{n-1/2}(i, k) - H_y^{n-1/2}(i, k-1)] \quad (1)$$

$$E_z^n(i, k) = \frac{\epsilon}{\epsilon + \sigma\Delta t} E_z^{n-1}(i, k) + \frac{\Delta t}{(\epsilon + \sigma\Delta t)\Delta x} [H_y^{n-1/2}(i, k) - H_y^{n-1/2}(i-1, k)] \quad (2)$$

$$H_y^{n+1/2}(i, k) = H_y^{n-1/2}(i, k) - \frac{\Delta t}{\mu_0\Delta z} [E_x^{n-1}(i, k+1) - E_x^{n-1}(i, k)] \\ + \frac{\Delta t}{\mu_0\Delta x} [E_z^{n-1}(i+1, k) - E_z^{n-1}(i, k)] \quad (3)$$

where i and k are the cell numbers in the x and z coordinates, respectively, and n tags the time step

The time domain ground wave propagation over earth's surface is simulated in TDWP as follows:

- The propagation region (see Fig.1a) is much larger than the FDTD computation space. Therefore, the FDTD computation space covers this region like a moving computation sub-region.
- An N_x by N_z (number of transverse and longitudinal cells, respectively) FDTD computation space is terminated by perfectly matched layer (PML) blocks [15,16] from left ($z \rightarrow -\infty$), right ($z \rightarrow \infty$) and ($x \rightarrow \infty$) top. Any boundary condition (BC) can be simulated at $x=0$. For example, a perfectly electrical conductor (PEC) or a lossy ground termination may be used at the bottom.
- Taking $N_x = 500$ and $N_z = 500$ (total of 250,000 FDTD cells) corresponds to a $50\lambda_{\min} \times 50\lambda_{\min}$ (λ_{\min} : minimum wavelength) space with a typical $\lambda_{\min}/10$ spatial discretization.
- A source with a chosen spatial height distribution, and temporally pulsed so that it furnishes broadband information with a single simulation, is injected through the relevant field components.
- One-way propagation is traced via a 2D rectangular window as shown in Fig.1b. The content of this propagation window is the pulse, which carries information related to the three wave components; direct, ground-reflected and surface waves.
- This virtual propagation window moves from left to right in FDTD computation space and circulates back to the left when reaches the right most-end, which is the initial profile of the next FDTD computation space. The

process and FDTD simulations repeat until the wave longitudinally propagates to a desired range.

- Keeping in mind the number of FDTD cells traced during the circulation of the propagation window, the transverse and/or longitudinal propagation characteristics are obtained.

Since TDWP is based on sliding the rectangular FDTD window along the propagation direction, it is defined for the flattened earth. But, the effects of the earth's curvature may easily be added via the relative permittivity $\epsilon_r = n^2(x,z)$, as done in analytical approximate formulations [1], by modifying the refractivity profile. The earth's curvature can be included by defining the height profile of refractive index at a given range as $n = n_0 + x/a$ (where $a = 6378 \text{ km}$ is the earth's radius and n_0 is the refractive index value at the ground). This is valid when refractive index is constant. In real world, refractive index above the ground changes with both height and range. The change of refractive index with height is mostly dominant, since changes with range are relatively much slower. Therefore, only vertical refractive index profiles are of interest for most of the propagation cases.

Because of the closeness of n to unity, it is customary to use the refractivity N defined as

$$N = (n(x) - 1) \times 10^6. \quad (4)$$

N is dimensionless, but is measured in "N units" for convenience. N depends on the pressure P (mbar), the absolute temperature T ($^\circ\text{K}$) and the partial pressure of water vapor e (mbar) as [17],

$$N = 77.6 \frac{P}{T} + 3.73 \times 10^5 \frac{e}{T^2} \quad (5)$$

which is valid in earth-troposphere waveguides and can be used in ground wave propagation modeling. Depending on the variation of P , T and e , various vertical refractivity profiles are defined. It has been found that refractivity gradient with respect to height is around -40 Nunit/km (i.e., $\partial N / \partial x = -40 \text{ Nunit/km}$) after long period of measurements and observations around the world. This is accepted as *standard atmosphere* profile.

If the refractive index were constant, radio waves would propagate in straight lines. Since n decreases with height (e.g., as in the standard atmosphere case), radio waves are bent downward towards the earth, so that the radio horizon lies further away than the optical horizon.

In TDWP (and also in other wave propagators, such as SSPE) it is easy to include both the earth's curvature and the standard atmosphere condition at once by using $n=n_0+x/a_e$, where $a_e=4a/3=8504\text{km}$ is the effective earth's radius.

In summary, n is either defined as $n=n(x)+x/a$, in order to take into account the effects of earth's curvature for all variations of atmospheric refractivity index, or equivalent fictitious medium is introduced, where N as defined in (4) is replaced by the modified refractivity M

$$M = N + \frac{x}{a} \times 10^6 = N + 157x \quad (6)$$

with the height x given in kilometers [17]. N decreases by about 40Nunit/km while M increases by about 117Nunit/km for standard atmosphere. Sub-refraction (super-refraction) occurs when the rate of change in N with respect to height (i.e., $\partial N / \partial x$) is less (more) than 40Nunit/km.

The direct, ground-reflected and surface waves are traced in time domain, where wave fronts and their interferences (wave maxima and minima) appear as 2D images. A typical example is given in Fig.2 for a bilinear refractivity profile. Here, equi-amplitude contours are plotted as height versus range. A Gaussian altitude profile is fed as the initial field distribution inside a 500×500 FDTD computation space corresponding to $50\text{m} \times 50\text{m}$ physical space. The initial field distribution has a pulse character in time (i.e., first derivative of a Gaussian function with 200MHz bandwidth at 100MHz center frequency). A 500×250 virtual window circulates 20 times as if the longitudinal number of cells in FDTD computation space is 5000. Instant snapshots are taken at different simulation times and are plotted as the field profiles at different ranges. As shown in the figure, the wave propagates towards the ground and reflects

back. The interference of direct and ground reflected waves as well as the surface waves are clearly observed in the figure.

Time histories of the pulse propagation in Fig.2, accumulated at different ranges and along the source height (i.e., 25m above the ground) is shown in Fig.3. The four plots, arranged in two vertical columns, correspond to the 94ns time histories (i.e., signal vs. time) at four different ranges (noted on the top right of each plot). These plots also correspond to the signal accumulation at four ranges inside nine FDTD propagation windows. Since the scale in each plot is normalized to its maximum value in order to reveal the detailed pulse shapes along the entire trajectory, relative field strengths with respect to the first window are also included as dB values inside the boxes. At $z=Z_1=24\text{m}$, only the initial pulse appears inside the 94ns FDTD propagation window because the delay of the signal caused by the path difference R_1-R_2 exceeds the window length. As the distance increases the path difference R_1-R_2 decreases and the ground-reflected pulse also appears inside the 94ns FDTD propagation window (see Figs.3b and 3c). Inside the last FDTD window (at $Z_4=223\text{m}$) the direct and ground-reflected pulses are almost indistinguishable. The signal in the last window is 13dB weaker than the signal in the first window.

Frequency domain characteristics can easily be obtained from the FDTD simulations. For example, an altitude field distribution at a given range can be obtained as follows:

- FDTD simulation is performed as explained above and propagation of waves is traced with the sliding rectangular window until the desired range.
- Time domain propagation data is accumulated at a number of altitude points (L) at the desired range (as given in Fig.3). A 2D array is used to accumulate the transient responses for all altitude points at the desired range.
- The accumulation continues until all the transients disappear at all altitude points and L different plots (each of which looks like the one shown in one of the windows of Fig.3) are obtained.
- After the FDTD simulation, altitude field distribution at any frequency (within the content of the pulse) is obtained by applying off-line DFT analysis to time histories at each altitude point.

Modeling ground wave propagation with TDWP needs careful parameter selection. First of all applying PML absorbing boundary simulators for backward as well as upward propagated waves is a challenging signal processing problem. Effective absorption within PML blocks depend on the number of PML layers and artificial PML medium parameters, which in turn depend on the wave phenomena inside the moving FDTD window. For a chosen number of PML blocks and artificial medium parameters, different degrees of absorption are obtained for surface guided, anti-guided, elevated ducted and/or rough surface scattered wave components. Therefore, one should be aware of possible induced wave components before the application of TDWP. This can also be obtained by visualizing the time domain propagation within the chosen scenario and by observing the real time pulse propagation. It should also be noted that, for long-range with dominant forward scattered propagation, the wave turns out to be plane (as expected in the far field), where the direction of propagation is parallel to the PML blocks, which is the worst case for PML absorbing boundary simulations and is a challenging problem. Nevertheless, TDWP with well-chosen PML parameters is an effective propagation simulator as presented in this paper.

Secondly, the numerical dispersion effects should be taken into account when dealing with long-range propagation scenarios. The longer the range the more spatial dispersion. Since TDWP is based on the application of 2D moving FDTD window, simulation of two-way propagation together with surface-scattered waves is possible. Therefore, there are forward, backward and/or upward propagated wave components inside the sliding FDTD window. This requires an intelligent separation of forward propagated pulse from the backward and upward propagated pulses. This separation and spatial dispersion can be controlled by applying a dynamic FDTD window size instead of a fixed-one.

III. The Frequency-domain Wave Propagator (SSPE)

SSPE is a frequency domain wave propagator, which is the solution of a parabolic type (PE) wave equation [6-8]. If the propagation medium is assumed to be homogeneous with the refractive index n , field components satisfy the 2D scalar wave equation. This is useful for mostly propagation in troposphere where the range and

height variations of n is slow on the scale of wavelength. In order to solve 2D wave equation, a field function $\varphi(z,x)$, which varies slowly in range for energy propagating at angles close to the paraxial direction, is taken into consideration [18].

$$u(z, x) = e^{-ikz}\varphi(z, x) \quad (7)$$

where x and z are the height and range variables, respectively, and k is the free-space wavenumber. Then the 2D wave equation can be split into backward and forward propagating waves as

$$\frac{\partial u}{\partial z} = -ik(1 + Q)u \quad (\text{backward}) \quad (8)$$

$$\frac{\partial u}{\partial z} = -ik(1 - Q)u \quad (\text{forward}) \quad (9)$$

where

$$Q = \sqrt{\frac{1}{k^2} \frac{\partial^2}{\partial x^2} + n^2(z, x)} \quad (10)$$

is the pseudo-differential operator. The standard parabolic equation for forward propagation can be derived using first-order Taylor expansions of the square root and exponential functions [18],

$$\frac{\partial^2 u}{\partial x^2} + 2ik \frac{\partial^2 u}{\partial z} + k^2(n^2 - 1)u = 0 . \quad (11)$$

The solution of (11) with the help of Fourier transform is called SSPE, which is a one-way propagator that is valid under paraxial approximation (i.e., under weak longitudinal refractivity dependence or near axial propagation), where backscatter effects are omitted. The general solution of the SSPE technique is given as;

$$u(z, x) = \exp\left[i\frac{k}{2}(n^2 - 1)\Delta z\right] FFT^{-1}\left[\exp\left[-i\frac{k_x^2 \Delta z}{2k}\right] FFT\{u(z_0, x)\}\right] \quad (12)$$

where $\Delta z = z - z_0$, k_x , FFT and FFT⁻¹ correspond to range step size, transverse wavenumber, discrete (fast) Fourier and inverse discrete (fast) Fourier transforms, respectively. The standard PE technique is a narrow-angle propagation approximation because the error caused by using first-order Taylor expansions is based on the angle of the wave from the horizontal. Since higher order polynomial expansions of the square root results in instability [19,20], other types of approximations, which include Padé-(1,1) expansion are used in order to solve wide-angle propagation problems [21]. In this paper, standard PE solution, which is satisfactory for the examples, has been used.

Since PE is an initial value problem, an initial transverse field distribution, $u(z_0, x)$ is injected and is longitudinally propagated through a medium defined by its refractive index profile $n(z, x)$; then the transverse field profile $u(z_0 + \Delta z, x)$ at the next range step, is obtained. By multi-moving back and forth between x and k_x domains via FFT and inverse FFT the transverse field profile at any range may be obtained.

The 2D SSPE propagation space is pictured in Fig.4. The implementation of the SSPE algorithm is as follows:

- An altitude profile is injected into the SSPE wave propagator. A 1D complex array is used to built the initial profile $u(z_0, x_i)$, where x_i ($i=1, \dots, L$, L is number of altitude points). This array contains amplitude and phase of the fields at each altitude (see Fig.4a).
- SSPE can not handle the BC at the surface by itself. Dirichlet or Neumann type BCs can be satisfied by either extending initial vertical profile from $[0 - X_{\max}]$ to $[-X_{\max}, X_{\max}]$, odd or even symmetric, or by applying SINE or COSINE FFT, respectively (see Fig.4b). In this paper, we use Neumann type BC that is required for a vertical polarization problem.
- This initial profile is longitudinally propagated from z_0 to $z_0 + \Delta z$ via eq.(12). The same complex array is used to store the altitude profile at the next range step.
- Using the new altitude profile as the initial profile for the next step and applying SSPE propagator for the second time yield the altitude profile at the second range step $z_0 + 2\Delta z$ (see Fig.4c).

- The procedure is applied repeatedly until the propagator reaches the desired range z_{last} .
- The transverse and longitudinal step sizes (Δx and Δz , respectively) and maximum altitude X_{max} are determined from the wave content and wavenumber requirements as well as sampling necessities and aliasing effects[6-8].

Two typical transverse refractivity profiles and SSPE propagation simulations through the ducts formed by these refractivity profiles are pictured in Fig.5. On top of the figure, a surface duct (i.e., a standard linearly decreasing refractivity over flat earth) and propagation of transmitted signal, which has a Gaussian height profile, is plotted. At the bottom, an elevated duct formed by a tri-linear vertical refractivity (over spherical earth) and its effect on propagation is plotted. As long as trapped within paraxial region, propagation through any duct formed by any transverse and/or longitudinal refractivity variation can be modeled via the SSPE propagator.

Terrain implementation, which is important for propagation prediction, is not very difficult for SSPE algorithm. There are different types of terrain modeling and it is possible to choose the appropriate one for the problem. One of them is called as conformal mapping [18,22], which depends on the change of variables due to terrain height. If the terrain function is known, it is easy to apply this conformal mapping to the SSPE algorithm since only the second derivative of the function is required for terrain inclusion in refractive index. Generally, it is not possible to know the terrain function, instead, the ground height difference with range can be measured, therefore there exist only the terrain height for each range step. With the help of this knowledge, terrain can be represented as a sequence of linear segments. Then, the second derivative can be determined using second-order central difference formula with the range interval corresponding to the PE range step for the SSPE algorithm [18,22].

Another simple way of terrain modeling is called as staircase terrain modeling [18], where slope values are not required, only the terrain height for each range is needed. For staircase terrain, the field is propagated in the usual way on each segment of constant height, applying the boundary condition at the ground. When the terrain

height changes, corner diffraction is ignored since paraxial approximation neglects backscatter so the field is simply set to zero on vertical terrain facets, which is suitable for the assumption that the ground does not support propagation [18]. Since the computation height is not changed due to the terrain, there is no need for the modification of refractivity index gradient, therefore it is also easy to implement the staircase terrain modeling into the SSPE algorithm.

IV. Numerical Applications

To check the validity of the new time-domain wave propagator and to make comparisons between TDWP and SSPE, a surface duct problem is taken into account. A linearly decreasing refractivity altitude profile (e.g., standard atmosphere without earth's curvature) corresponds to a surface duct over planar earth's surface. The earth's curvature may also be included as a perturbation in refractivity as explained in Section II.

First, one-way propagation through a strongly trapping surface duct over flat earth is simulated with both TDWP and SSPE and the results are compared against each other. Same transverse (spatial) initial profile is fed into both TDWP and SSPE algorithms and the propagators are run for 500m. The TDWP is used once and broad band results are obtained. The SSPE propagator needs to be run separately for each frequency. Vertical field profiles at 500m away from the transmitter, which are obtained with both techniques are plotted in Fig.6 as propagation factors ($|E/E_0|$) vs. height. A similar procedure is applied to calculate the propagation factor in both TDWP and SSPE techniques. Both algorithms are run twice. In the first runs, propagation over PEC ground is simulated. In the second runs, they are repeated in free-space and the propagation factors are obtained. A good agreement between the results of time and frequency domain wave propagators is clearly seen from the figure.

A similar comparison is given in Fig.7 for range variation of vertical electric field component at a fixed altitude. In this case, time histories of propagation at various observation ranges at 25m fixed altitude are accumulated in TDWP and off-line DFT is then applied. SSPE calculates fields at all altitudes of all ranges, therefore, the

calculation procedure does not change. In fact, higher range steps can be used in SSPE, but small steps are chosen for the comparison of range variations. The results agree quite well for both 100MHz (bottom) and 150MHz (top) frequency calculations. As seen from both Figs.6 and 7, interaction of direct and ground reflected wave components increases as the frequency increases.

First calculations and comparisons presented above belong to surface duct over flat earth. The calculations are repeated when earth's curvature is taken into account. In both TDWP and SSPE techniques, propagation over spherical earth's surface can be modeled as a modification in vertical refractivity profile. Guiding over flat earth's surface is modeled by a negative vertical refractivity gradient. On the other hand, it becomes a positive refractivity gradient when the curvature is included. While waves are trapped over surface with negative vertical refractivity gradient, energy detaches from the surface (i.e., wave divergence occurs) for positive vertical refractivity gradient.

In Fig.8, two typical SSPE results are pictured. Again, equi-amplitude contours are plotted as height versus range. The initial field profiles are normal modes [3,5] at 3MHz and 10MHz, where field maxima point the surface. They are the eigensolutions of 2D scalar Helmholtz wave equation with Neumann type BC at the surface (surface modes). Therefore, initial profiles simulate the surface coupling of transmitter energy. As SSPE proceeds, the detachment of the energy from the surface occurs, which is clearly observed in the figure. Although most of the energy detaches from the surface significant energy still follows the curvature of the earth through the shadow region up to 500km. Surface wave propagation at 3MHz is more significant than at 10MHz.

This anti-guiding problem is also modeled via TDWP and similar detachment is observed in time domain. Time domain propagation over spherical earth's surface is plotted in Fig.9. As TDWP proceeds, the pulse detaches from the surface and energy over the surface diminishes with range.

The results of TDWP and SSPE for this anti-guiding model are compared in Fig.10. Here, propagation factor vs. height at three different frequencies at 500m range are shown. As clearly seen from the figure, the higher the frequency the stronger the wave

detachment from the surface. The propagation factor just above the surface at 500m range is -22dB at 100MHz and reduces to -33dB at 200MHz . This means, when the frequency increases from 100MHz to 200MHz field amplitude just above the surface at the same range reduces by 11dB .

Finally, the terrain effects at HF frequencies are shown in Fig.11 for three frequencies. At the top, a typical terrain model that can be accepted as two mountains with a valley in between is shown. At the bottom, range variations of the propagation factor are plotted for $5, 15$ and 30MHz . Here, to calculate the propagation factor SSPE is run twice and in the first run, propagation over PEC terrain is simulated. In the second run, it is repeated for PEC ground without terrain and the propagation factor, which includes only the terrain effects, is obtained. In fact, in order to simulate propagation for terrain at HF frequencies, mixed boundary conditions for ground should be applied. Here, Neumann boundary condition is used since our aim is to show only the terrain effect variations at different HF frequencies. As it is seen from the figure, the terrain affects propagation much more while frequency increases.

The TDWP is computationally expensive, when compared to the SSPE propagator. Although the TDWP simulation time is much more than the other, the SSPE algorithm must be repeated for hundreds of times to give the broad band propagation information obtained with one TDWP run. It should be noted that, no parameter optimization or algorithmic arrangement has yet been done in TDWP algorithm. Its memory requirements and computation time will drastically be decreased when optimization is done and when the sliding window size is dynamically controlled.

V. Conclusions

Two powerful propagators are taken into account in this paper. The SSPE has been in use for more than a decade and has successfully been applied to many one-way propagation problems including acoustics, electromagnetics and optics. On the other hand, TDWP has just been introduced [9] and applied to various electromagnetic ducting problems. A very similar FDTD based technique has also been used in analyzing VLF and LF propagation through earth – ionosphere waveguides [23].

The new time domain wave propagator, TDWP is very promising in dealing with various complex propagation problems. Since not restricted within paraxial region, TDWP seems to have more potential than SSPE in modeling propagation problems. Terrain effects and surface roughness as well as ground losses [24-25] can be modeled, where any kind of transverse and/or longitudinal refractivity profiles can be taken into account [26,27]. The technique may also be applied to vertical propagation [28] or any other waveguiding structures [29].

Although short-range calculations are performed in the numerical examples presented here, theoretically there is no altitude or range limitations or BC restrictions at the surface in TDWP applications. Long computation times may be required for long range propagation simulations, which may be overcome by using some intelligent algorithmic and/or parallel processing techniques. It should be noted that, signal processing aspects during TDWP application are very important. One should be aware of the necessity of:

- monitoring the forward propagated and/or upward wave components and controlling its dispersion both in time and spatial domains,
- separation and absorbing of the backward and/or upward propagated or scattered wave components,
- absorbing surface scattered and/or anti-guiding or anti-ducting wave components,
- taking care of numerical dispersion effects when long propagation regions are of interest,
- extra caution in applying PML absorbing boundary simulations when long range propagation with dominant forward scattered wave component is of interest.

Nevertheless, by adding decision-makers and parallel processing routines, TDWP may be able to simulate not only 2D but also 3D pulsed propagation, utilizing digital terrain data, which may include surface impedance variations.

References

- [1] L. Sevgi & L. B. Felsen, "A new Algorithm for Ground Wave Propagation Based on a Hybrid Ray-Mode Approach", *Int. J. of Numerical Modeling*, Vol 11, No 2, pp.87-103, 1998
- [2] L. B. Felsen & L. Sevgi, "Adiabatic and Intrinsic Modes for Wave Propagation in Guiding Environments with Longitudinal and Transverse Variations: Formulation and Canonical Test", *IEEE Transactions on Antennas and Propagat.* Vol 39 No 8, pp.1130-1136, 1991
- [3] L. B. Felsen & L. Sevgi, "Adiabatic and Intrinsic Modes for Wave Propagation in Guiding Environments with Longitudinal and Transverse Variations: Continuously Refracting Media", *IEEE Transactions on Antennas and Propagat.* Vol.39 No.8, pp.1137-1143, 1991
- [4] B. Polat, E. Topuz & L. Sevgi, "Wave Propagation Through Linearly Tapered Homogeneous Dielectric Slab Waveguides", *AEU, Int. J. of Electronics and Communication*, Vol.52, No.2, pp.105-108, March 1998
- [5] L. Sevgi, S. Paker & E. Topuz, "Intrinsic Mode (IM) Formalism and Its Asymptotical Evaluations in 3D Non-Homogeneous Environments", *AEU, Int. J. of Electronics and Communication*, V.50, No.3, pp.201-207, May 1996
- [6] G. D. Dockery, " Modeling Electromagnetic Wave Propagation in the Troposphere Using Parabolic Wave Equation", *IEEE Transactions on Antennas and Propagat.* Vol.36, pp.1464-1470, 1988
- [7] A. E. Barrios, " Parabolic Equation Modeling in Horizontally inhomogeneous Environments", *IEEE Transactions on Antennas and Propagat.* Vol 40, pp.791-797, 1992
- [8] L. Sevgi "Split Step Parabolic Equation Solutions in Surface Duct-to-Elevated Duct Transition", *Turkish J. of Physics*, Vol 19, No 3, pp. 541-551, 1995
- [9] F. Akleman & L. Sevgi, "A Novel Finite-Difference Time-Domain Wave Propagator", *IEEE Transaction on Antennas and Propagat*, Vol. 48, No 5, pp.839-841, May 2000
- [10] K. S. Yee, "Numerical solution of initial boundary value problems involving Maxwell's equations" *IEEE Transactions on Antennas and Propagat*, V-14, no. 3, pp. 302-307, 1966
- [11] L. Sevgi & S. Paker, "FDTD Based RCS Calculations and Antenna Simulations", *AEU, International J. of Electronics and Commun.*, Vol.52, No.2, pp.65-75, March 1998
- [12] F. Akleman & L. Sevgi, "Radar Cross Section and Antenna Modeling with FDTD Method", *Proc. of JINA'98, 10th Int. Symposium on Antennas*, November 17-19, 1998, France
- [13] F. Akleman & L. Sevgi, "FDTD Analysis of Human Head – Mobile Phone Interaction in Terms of Specific Absorption Rate (SAR) Calculations and Antenna Design", *Proc. of IEEE-APS, Conference on Antennas & Propagation for Wireless Comm.*, pp. 85-88, November 2-4, 1998, Waltham, MA, USA
- [14] M. Orhan Ozyalcin & L. Sevgi, "Comparisons of FDTD and TLM methods in Shielding effect analysis", *Proc. of IEEE CEFC'98 the Eight Biennial IEEE Conference on Electromagnetic field Computation*, June 1-3, Tuscon, Arizona, USA
- [15] J. P. Berenger, "A Perfectly Matched Layer for the Absorption of Electromagnetic Waves", *J. Comput. Phys.*, Vol.114, pp. 185-200, 1994
- [16] F. Akleman & L. Sevgi, "A Novel Implementation of Berenger's PML for FDTD Applications", *IEEE Microwaves and Guided Wave Letters*, Vol.8, No 10, pp.324-327, 1998

- [17] M. P. M. Hall, L. W. Barclay, M. T. Hewitt (ed), *Propagation of Radiowaves*, IEE Press, London, 1996
- [18] M. Levy, *Parabolic equation methods for electromagnetic wave propagation*, Institution of Electrical Engineers, 2000
- [19] A. Bambenger, B. Engquist, L. Halpern and P. Joly, "Parabolic Wave Equation Approximations in Heterogeneous Media", *SIAM J. Appl. Math.*, vol. 48, pp. 99-128, 1988
- [20] A. Bambenger, B. Engquist, L. Halpern and P. Joly, "Higher Order Paraxial Wave Equation Approximations in Heterogeneous Media", *SIAM J. Appl. Math.*, vol. 48, pp. 129-154, 1988
- [21] J. F. Claerbout, *Fundamentals of Geophysical Data Processing with Application to Petroleum Prospect*, McGraw-Hill, New York, 1976
- [22] A. E. Barrios "A Terrain Parabolic Equation Model for Propagation in the Troposphere", *IEEE Transactions on Antennas and Propagat.*, Vol. 42, No.1, pp.90-98, 1994
- [23] J. P. Berenger, "Finite Difference Computation of VLF-LF Propagation in the Earth – Ionosphere Waveguide", *Proc. Of URSI XXVI General Assembly*, pp. 464, Toronto, 1999
- [24] G. D. Dockery and J. R. Kuttler, "An Improved Impedance Boundary Algorithm for Fourier Split Step Solutions of the Parabolic Wave Equations", *IEEE Transactions on Antennas and Propagat.* Vol 44, No 12, pp.1592-1599, 1996
- [25] S. H. Marcus, "A Hybrid (finite difference-surface Green's function) Method for Computing Transmission Losses in an Inhomogeneous Atmosphere over irregular terrain", *IEEE Transactions on Antennas and Propagat.* Vol 40, No 12, pp.1451-1458, 1992
- [26] F. Akleman & L. Sevgi, "Realistic Surface Modeling in a Time-domain Wave Propagator ", *IEEE Transactions on Antennas and Propagation*, (submitted) July 2000
- [27] L. Sevgi, F. Akleman & L. B. Felsen, "Ground Wave Propagation Modeling: Problem-matched Analytical Formulations and Direct Numerical Techniques", *IEEE Antennas and Propagation Magazine*, (submitted) Sep. 2000
- [28] M. F. Levy, "Horizontal Parabolic Equation Solution of Radio Wave Propagation Problems on Large Domains", *IEEE Transactions on Antennas and Propagat.*, V-43, no. 2, pp. 137-144, 1995
- [29] L. Sevgi & E. Topuz, "Split step Parabolic Equation Analysis of Coupled Dielectric Waveguides", *ELEKTRIK, Turkish J. of Electronics and Communication*, Vol. 3, No 2-3, pp. 85-92, 1995

Figure Captions

Figure 1: (a) The 2D propagation space. Here, x and z are the transverse and longitudinal coordinates, respectively. A finite-sized FDTD computation space is used as if this region is covered by multi FDTD computation spaces. (b) Detailed sketch of one FDTD computation space. Left, right and top boundaries are terminated by PML blocks to simulate an open propagation region. The bottom is shown to be PEC in this example. A virtual propagation window, which is adjusted to contain the propagation of the initial pulse, slides from left-to-right inside this FDTD computation space. The final window of the current FDTD computation space will be the initial window of the next FDTD space.

Figure 2: Time-domain pulse propagation inside the sliding window at propagation ranges Z_1, Z_2, \dots, Z_6 . Z_1 : 670th time step $\approx 50\text{m}$ range; Z_2 : 1570th time step $\approx 110\text{m}$ range; Z_3 : 2250th time step $\approx 155\text{m}$ range; Z_4 : 2580th time step $\approx 180\text{m}$ range; Z_5 : 3070th time step $\approx 215\text{m}$ range; Z_6 : 4330th time step $\approx 305\text{m}$ range. The propagation region is characterized by a longitudinally homogeneous, bi-linear vertical refractive index profile with $dn/dx=10^{-3}$ [n unit/m]. The vertical distribution of the source is Gaussian with spatial extent $\approx 15\text{m}$ and maximum at 25m height. The temporal distribution is a differentiated Gaussian pulse with 200MHz bandwidth centered at 200MHz.

Figure 3: Time histories of the pulse in Fig.2 observed at different ranges along the source height 25m above the surface. Four plots (from top to bottom, left to right) correspond to the FDTD propagation windows (signal vs. time) at four different ranges (indicated at the top right of each plot). The temporal extent of the FDTD window is 94ns. Each plot is normalized to its maximum signal strength and the relative dB levels are given inside the boxes.

Figure 4: (a) The 2D propagation space that extends from $x=0$ to $x=X_{\max}$ vertically and from $z \rightarrow -\infty$ to $z \rightarrow \infty$ horizontally. (b) Initial altitude profile of SSPE wave propagator at the range of $z=z_0$. The Dirichlet or Neumann type boundary condition at the surface is satisfied by extending vertical profile odd or even symmetric with respect to $x=0$ axis. The initial field profile at $z=z_0$ is $u(z_0, x)$. (c) The next altitude profile at $z=z_0+\Delta z$ is $u(z_0+\Delta z, x)$ and is obtained via a single SSPE run. Using $u(z_0+\Delta z, x)$ at $z=z_0+\Delta z$ as a new initial profile will give the profile $u(z_0+2\Delta z, x)$ at $z=z_0+2\Delta z$ via the second SSPE run. The desired altitude profile at $z=z_{\text{last}}$ ($z_{\text{last}}=z_0+N\Delta z$, N number of consecutive SSPE runs) is $u(z_0+N\Delta z, x)$ and is obtained after N consecutive SSPE runs.

Figure 5: Two typical SSPE simulations; (top) propagation through a surface duct formed by the standard atmosphere (i.e., linearly decreasing vertical refractivity) (bottom) propagation through an elevated duct formed by a tri-linear vertical refractivity profile.

Figure 6: Propagation factor $|E/E_0|$ vs. height computed via both TDWP and SSPE propagators at 500m away from the source (corresponding to the ranges of 250λ , 330λ , 415λ at 150MHz, 200MHz and 250MHz, respectively). The vertical

distribution of the source is Gaussian with spatial extent $\approx 15\text{m}$ and maximum at 25m height. The TDWP initial profile is a once-differentiated Gaussian pulse with bandwidth 200 MHz at center frequency 200 MHz ; the SSPE propagator is run separately for each frequency. The propagation region is characterized by longitudinally homogeneous, linear vertical refractive index with $dn/dx = -10^{-7}$ [n unit/m].

Figure 7: Propagation factor $|E/E_0|$ vs. range computed via both TDWP and SSPE at fixed altitude, for the same scenario explained in Fig. 6. Both the transmitter and observation altitudes are same and are equal to 25m . Top: 150MHz , bottom: 100MHz .

Figure 8: Wave detachment over earth's surface, under standard atmosphere approximation when earth's curvature is included (SSPE results). Top: 3MHz , bottom: 10MHz .

Figure 9: Wave detachment over earth's surface, under standard atmosphere approximation when earth's curvature is included (TDWP results with fictitious refractivity and curvature; the on-surface source is Gaussian with spatial extent of $\approx 15\text{m}$ and a once-differentiated Gaussian temporal profile with 200MHz bandwidth at 200MHz center frequency. The propagation region is characterized by longitudinally homogeneous, linear vertical refractive index with $dn/dx = 10^{-3}$ [n unit/m]

Figure 10: Propagation factor $|E/E_0|$ vs. height computed via both TDWP and SSPE propagators at 500m away from the source (corresponding to the ranges of 166λ , 250λ and 333λ at 100MHz , 150MHz and 200MHz , respectively). On-surface source is Gaussian with spatial extent of $\approx 15\text{m}$. In TDWP, a once-differentiated Gaussian temporal profile with 200MHz bandwidth at 200MHz center frequency is used. The SSPE propagator is run separately for each frequency. The propagation region is characterized by longitudinally homogeneous, linear vertical refractive index with $dn/dx = 10^{-3}$ [n unit/m].

Figure 11: (Top) A typical terrain model with two mountains and a valley lying between them. **(Bottom)** Propagation factor results for three frequencies $5, 15$ and 30MHz for this terrain type. Refractivity index for standard atmosphere that includes earth's curvature is used.

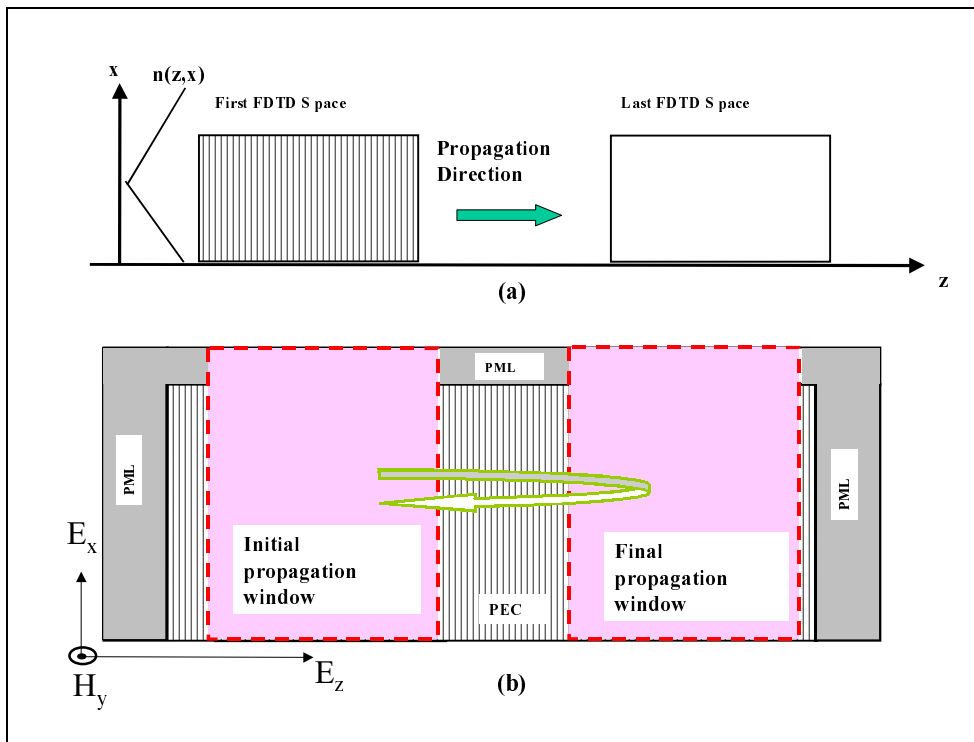


Figure 1:

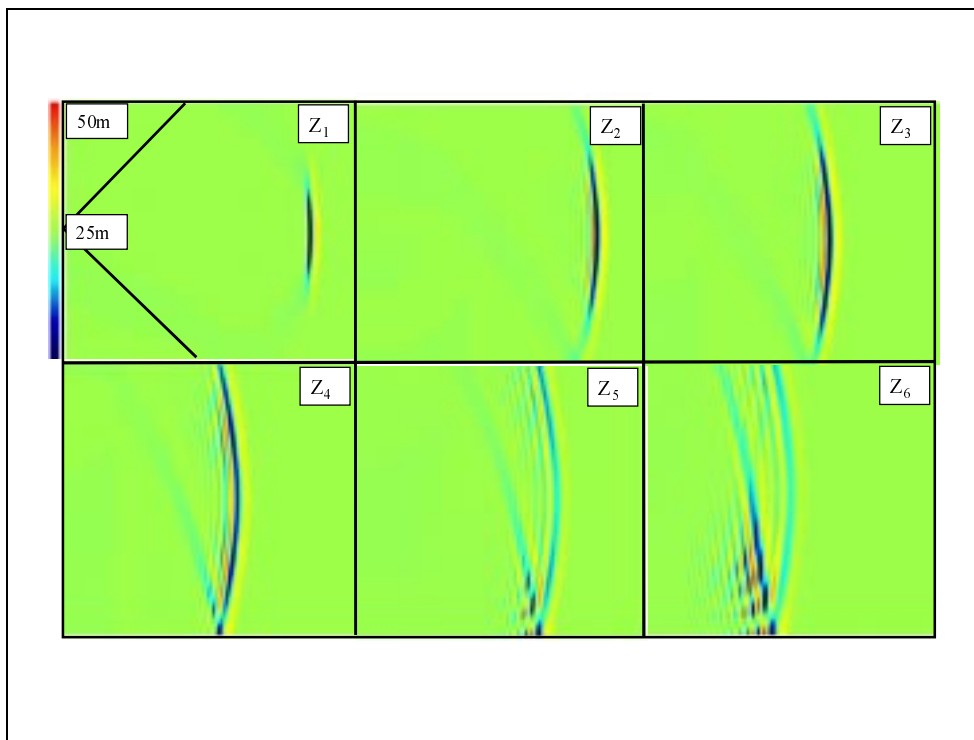


Figure 2:

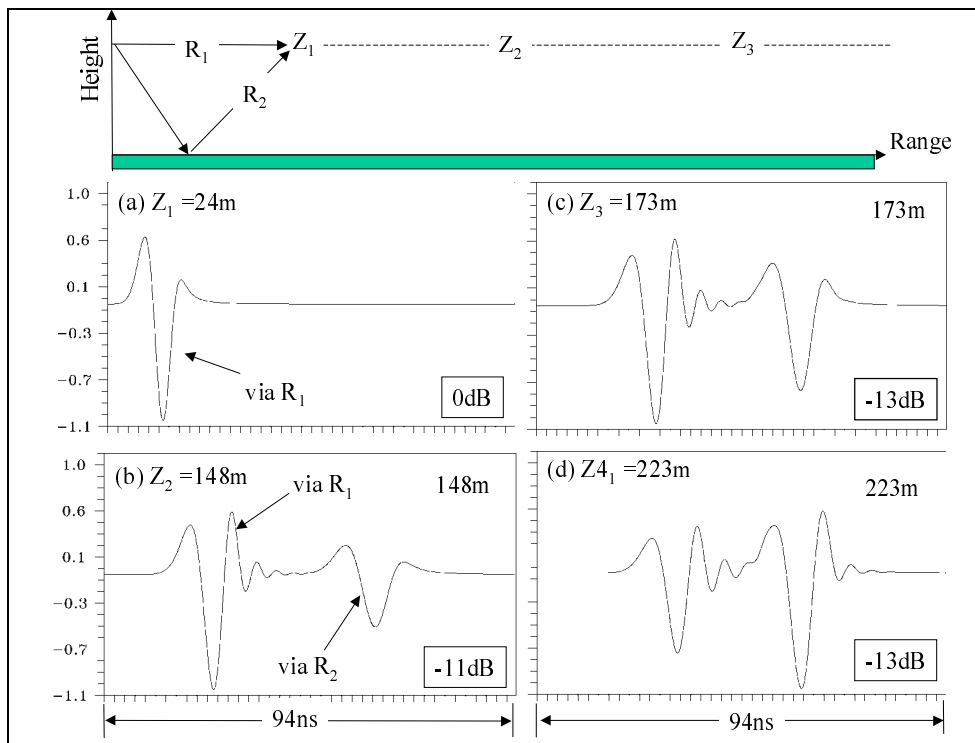


Figure 3:

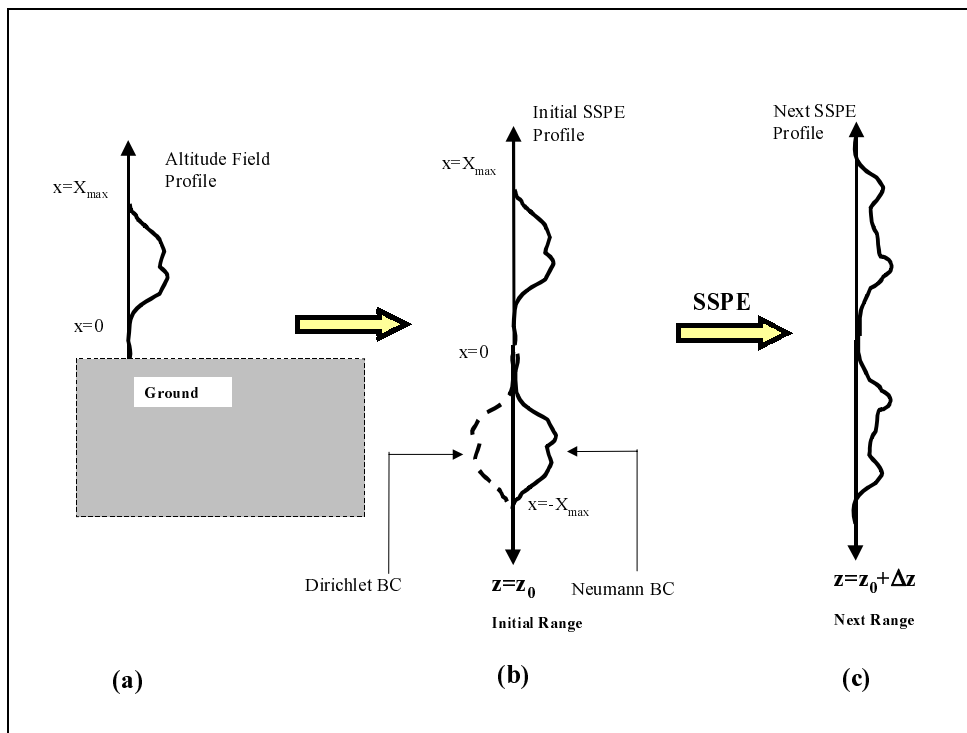


Figure 4:

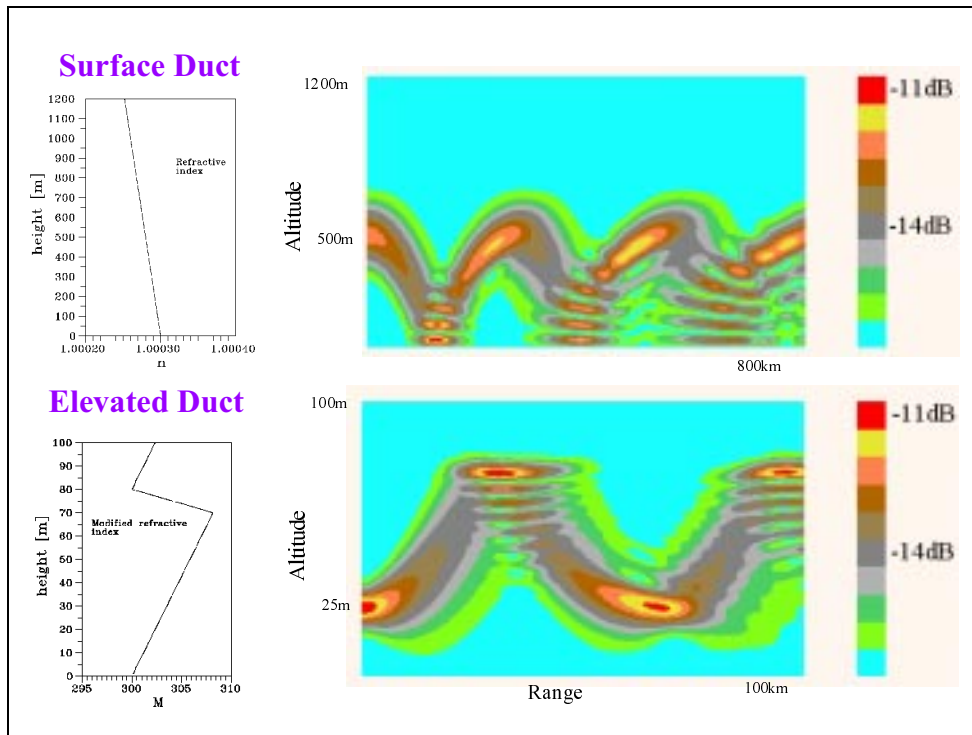


Figure 5:

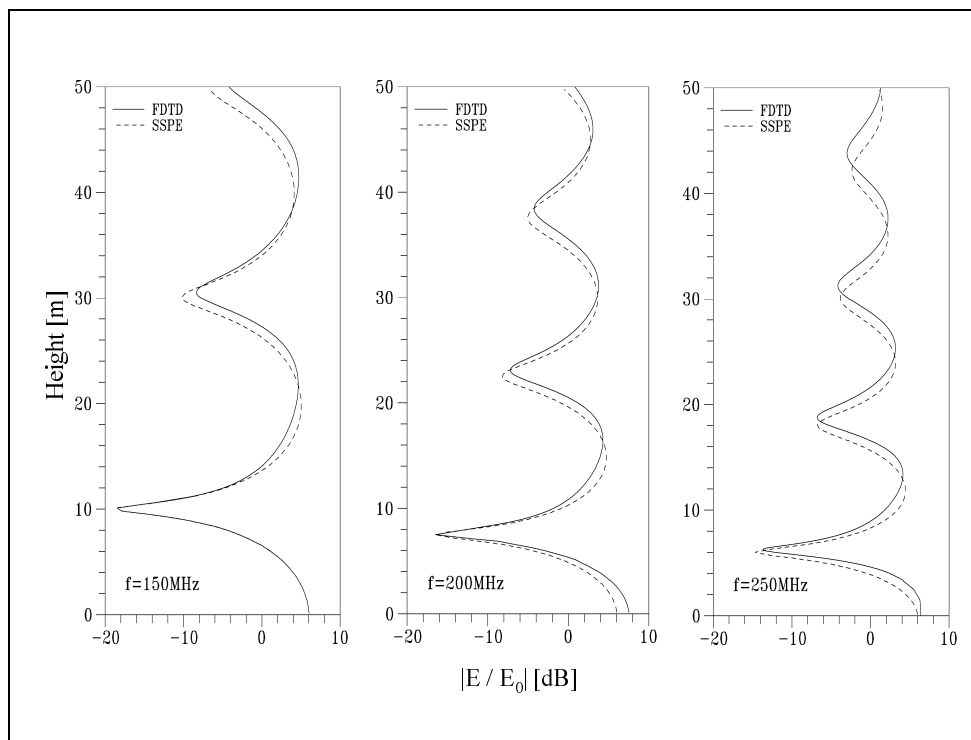


Figure 6:

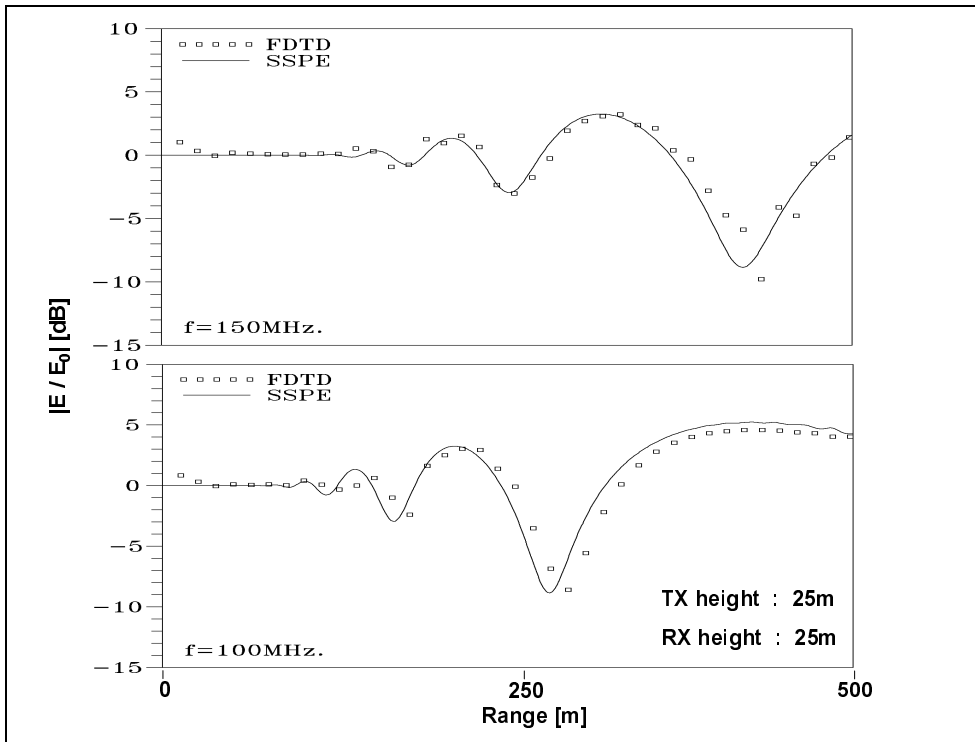


Figure 7:

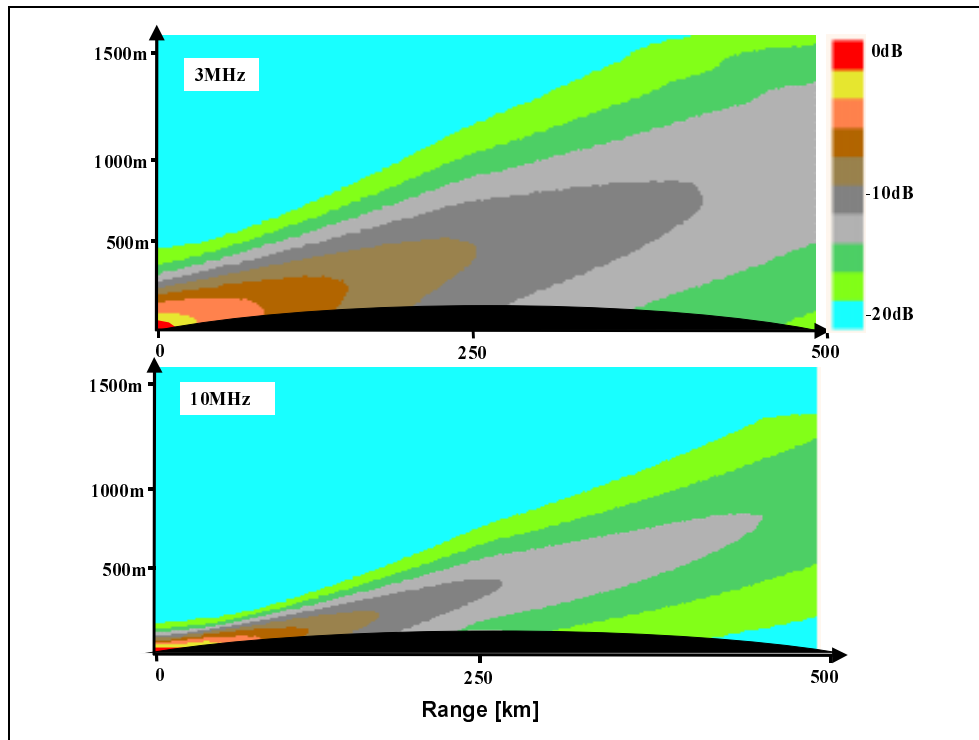


Figure 8:

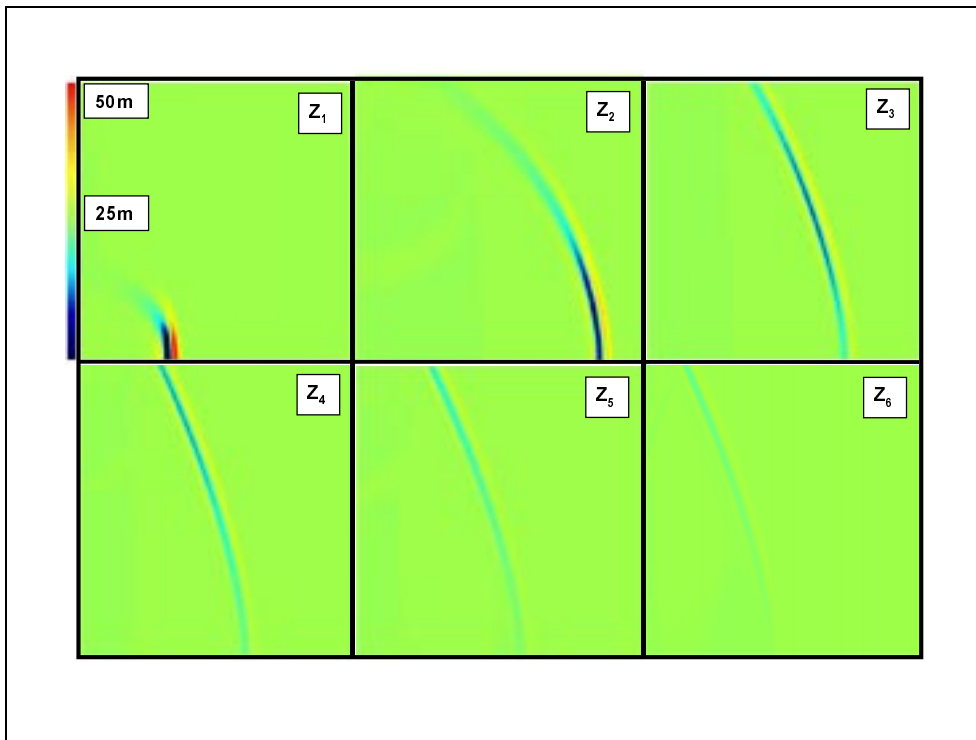


Figure 9:

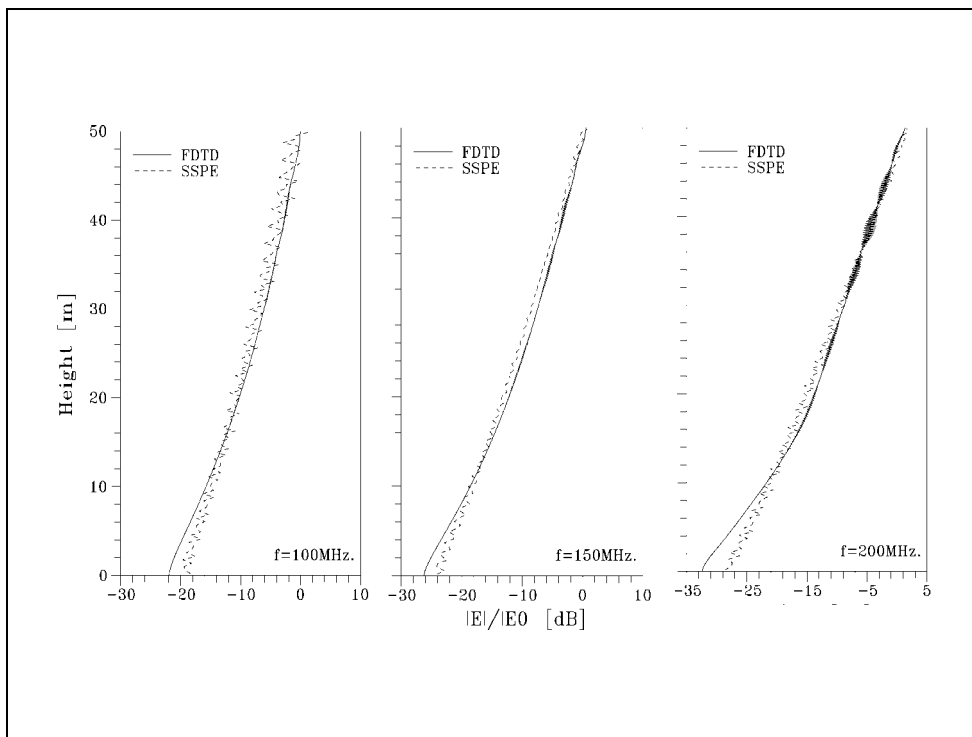


Figure 10:

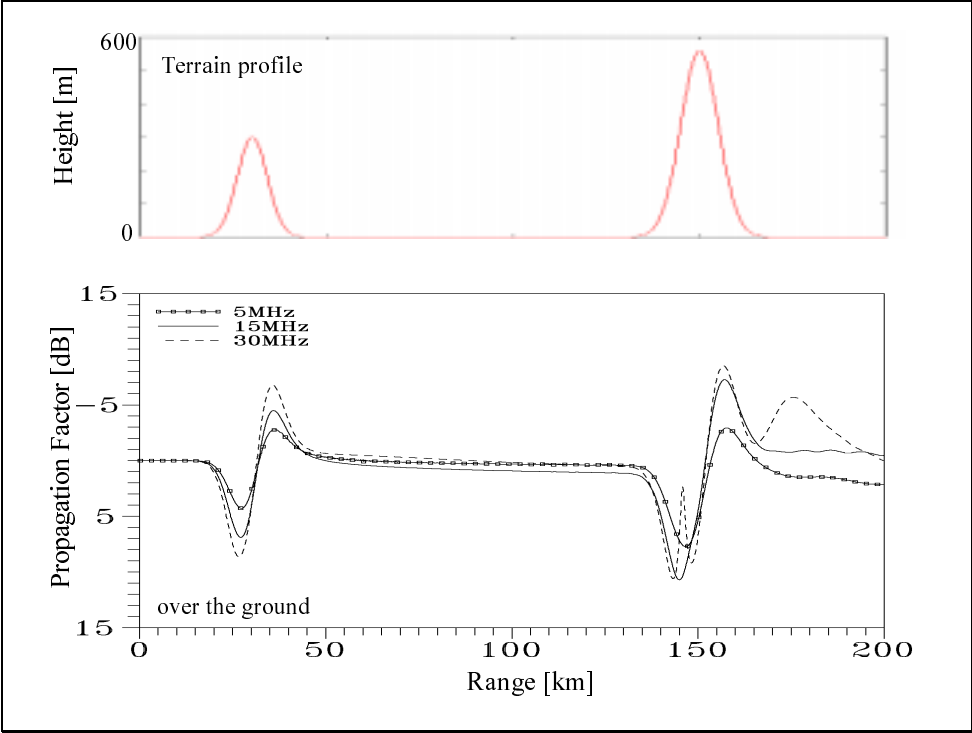


Figure 11: